iWood: Makeable Vibration Sensor for Interactive Plywood

Te-Yen, Wu
Dartmouth College
te-yen.wu.gr@dartmouth.edu

Xing-Dong Yang
Simon Fraser University
xingdong_yang@sfu.ca

ABSTRACT

iWood is interactive plywood that can sense vibration based on triboelectric effect. As a material, iWood survives common woodworking operations, such as sawing, screwing, and nailing and can be used to create furniture and artifacts. Things created using iWood inherit its sensing capability and can detect a variety of user input and activities based on their unique vibration patterns. Through a series of experiments and machine simulations, we carefully chose the size of the sensor electrodes, the type of triboelectric materials, and the bonding method of the sensor layers to optimize the sensitivity and fabrication complexity. The sensing performance of iWood was evaluated with 4 gestures and 12 daily activities carried out on a table, nightstand, and cutting board, all created using iWood. Our result suggested over 90% accuracies for activity and gesture recognition.

CCS CONCEPTS

• **Human-centered computing**; • **Human computer interaction (HCI)**; • **Interaction devices**;

KEYWORDS

Interactive wood, makeable sensor, vibration sensing

1 INTRODUCTION

The vision of ubiquitous computing heralds the future of smart home and work environments that can better understand and fulfill people's needs [42]. However, this vision is still far from reality as most things in today's world are not computing-powered, such as furniture made of wood or garments made of fabric. To allow computation and interactivity to better blend into everyday contexts, researchers have investigated ways to imbue them into everyday materials, of which, daily objects are made [3]. This way, the world made of interactive materials becomes interactive automatically while still being able to preserve the look and feel of its non-computational counterparts. Innovations like interactive
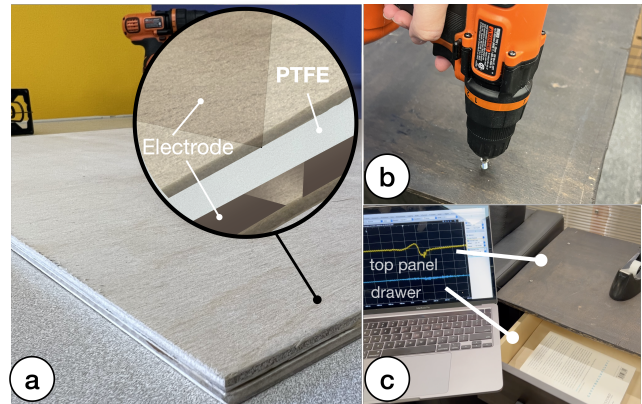
Figure 1: (a) iWood is interactive plywood that can be used as a vibration sensor to detect user input and activities. (b) A nightstand can be created using iWood using established woodworking operations like screwing. (c) iWood sensor remains functional even a part of it is damaged by the screws.

paper [6, 13, 19] and fabric [12, 30, 32, 33, 46, 47] all exemplify such efforts.

In this paper, we present a new type of interactive material created based on plywood, a type of wood commonly used in furniture, artifacts, floors, and building infrastructures. Beyond what plywood offers as a material, our prototype (called iWood) detects the subtle vibrations caused by users' gestures and activities based on the triboelectric effect [52]. iWood is makeable, meaning that it can be sawed, nailed, or screwed together to make smart objects (Figure 1b). Things created using iWood inherit the material's sensing capability and can detect a variety of user input and activities based on their unique vibration patterns. For example, a smart desk made of iWood can detect and log the user's work activities, such as writing and erasing, enabling new applications for skill development or personal reflection.

We implemented our prototype using a layer of triboelectric material sandwiched between two layers of electrodes, each attached to a plywood substrate (Figure 1a), similar to the structure commonly used in triboelectric nanogenerators (TENG) [21]. The electrode layers of iWood were uniquely designed to stagger with each other to only cover a separate part of the sensing area. This way short-circuiting caused by metallic screws and nails can be significantly reduced. Through a series of machine simulations and experiments, we carefully chose the size of the electrodes, the type of triboelectric materials, and the bonding method of the sensor layers to optimize the sensitivity and fabrication complexity of iWood. In a controlled experiment, we measured the sensing performance of the table, nightstand, and cutting board made of iWood over four input gestures and 12 common work and kitchen activities

(e.g., writing on a table). Our results suggested that in many tested conditions the smart items achieved a recognition accuracy of over 90%.

The key contributions of this work are in (1) a makeable plywood sensor that can be used to create smart wooden objects to sense user input and activities using vibration sensing; and (2) the usage scenarios demonstrating unique applications enabled by iWood as interactive material.

2 RELATED WORK AND BACKGROUND

We discuss work related to input on interactive fabric and paper, interactive wooden artifacts, cuttable sensors, and vibration sensing based on the triboelectric effect.

2.1 Input on Interactive Fabric, Paper, and Wooden Artifacts

fabrics have been instrumented with sensors to enable a wide variety of applications through sensing touch input [31, 32], mid-air hand gestures [46], deformation of the fabric [30, 31], and different types of objects that are in contact with the fabric [12, 47, 48]. For instance, Project Jacquard [32] is a new type of conductive yarn that can be woven into textiles to sense touch input. Aside from sensing user input, object recognition techniques have also been explored in interactive fabrics. For example, Capacitivo [47] can detect non-metallic objects, such as food using capacitive sensing.

In addition to interactive fabric, paper has been augmented with sensing capabilities to detect touch input [13, 19, 27], finger rubbing [19], the proximity of the hand [13], the shape of the paper [44], the deformation of the paper [13], and even sound [5, 6]. For example, PrintSense introduced a new pattern of printed conductive electrode arrays on paper to support multimodel interactions [13]. Paper generators leveraged the triboelectric effect to enable interactions like touch, rubbing, and sliding in a children's storybook [19].

Research on wooden artifacts has primarily focused on attaching sensing devices to off-the-shelf furniture or artifacts made of wood [15, 18, 26, 28, 29, 39, 49] rather than developing wood into an interactive material. Examples of this body of research include tables, walls, and floors instrumented with vibration sensors to detect touch or gesture events [15, 29, 49], people falling on the floor [10], user activities (e.g., cutting, typing, walking) [39], and the presence of some of the daily items on a table (e.g., glass, phone, coil, paper cup) [26]. Although it is an effective way to bring interactivity to the existing environment, the attached sensors and devices often do not blend well into the traditional aesthetics of wooden objects.

2.2 Cuttable Sensors

Sensor makeability is not entirely new. Our research was inspired by the line of work investigating cuttable sensors for rapid prototyping. An early example of cuttable sensors is Wimmer et al. [45] and Holman et al. [17] 's touch sensing strip that can be cut into different lengths to satisfy the needs of different applications. Similarly, Dementyev et al.'s sensor tape can also be cut into different lengths and is capable of measuring the proximity of nearby objects [9]. Beyond cutting in a 1D space, Olberding et al.'s touch sensor can be cut out in 2D shapes [27]. Built on top of this work, Takahashi

et al. [40] developed a cuttable coil grid for wireless power transfer using a method based on H-tree.

2.3 Vibration Sensing based on the Triboelectric Effect

Our sensing technique is based on the triboelectric effect and particularly triboelectric nanogenerator (TENG), which is a technology developed based on the principle of triboelectrification and electrostatic induction. It converts mechanical energy to a correlated electrical response and has been widely used in energy harvesting applications due to its high efficiency for energy transfer at low frequencies [21]. For example, Hao el al. [14] proposed a wood-based triboelectric nanogenerator (W-TENG) to power electronic devices. Sun et al. [38] improved W-TENG to harvest more energy by using a triboelectric material made of chemically functionalizing wood. Methods based on the triboelectric effect have also been used for sensing in a wide variety of applications to detect mechanical motion such as pressure [25, 51], vibrations [6, 7, 50], speed of wind [4], rotation of a disk [24], and acceleration of an object [53]. This method was also used as a sensing mechanism to instrument floors and tables to detect user activities, such as falling [36]. In comparison to other types of vibration sensors, such as piezoelectric ceramic or PVDF poled piezoelectric film, techniques based on triboelectrification are cheaper and easier to implement [6], thus making them suitable for plywood, especially for development at scale.

3 VIBRATION SENSING PRINCIPLE

iWood's sensing technique is based on the triboelectric effect caused by the contact and separation of a positive and negative triboelectric material (layer) [52]. When the two layers are pushed to contact with each other, the negative triboelectric layer gains electrons from the positive triboelectric layer, becoming negatively charged. The positive triboelectric layer becomes positively charged. When the subsequent propagation of vibrations separates the two triboelectric layers, a potential difference is induced between the electrodes connected to them. This causes the current to flow from the electrode of the positive triboelectric layer to the electrode of the negative triboelectric layer (with the presence of an external load between the two electrodes). When the two triboelectric layers are pushed towards each other again, a current flow in the reversed direction occurs, which completes the cycle of electricity generation. Even if the contact and separation take place at a micro-scale, the voltage signals generated by the triboelectric effect can still be measured for sensing purposes.

In general, the sensitivity of iWood is determined by (1) the maximum distance between the triboelectric layers when they are pushed away from each other due to vibration and (2) the surface charge density of the triboelectric layers [54]. The separation distance is determined by how tightly the triboelectric layers are bonded to each other. The surface charge density is determined by the material choice of the triboelectric layers. Materials with a stronger tendency to be negatively or positively charged lead to better surface charge density. For the negative triboelectric layer, polytetrafluoroethylene (PTFE) film is widely used [54]. For the positive triboelectric layer, there is a wider range of options with the most

common ones including wood, copper, nylon, and polyurethane (PU) [54].

4 MAKEABILITY ISSUE

The triboelectric vibration sensor can be implemented with a thin polytetrafluoroethylene (PTFE) film, sandwiched between two layers of copper film, each attached to a substrate of plywood board (Figure 2). In this implementation, one of the copper films not only serves as an electrode but also acts as the positive triboelectric layer [52, 54]. This copper film needs to be loosely attached to the PTFE film (e.g., along its edges) to allow space between them for bouncing. Note that the other copper film, which serves only as an electrode, needs to be glued completed to the PTFE film. This is required to limit the occurrence of triboelectrification only on the opposite copper film to maximize signal strength.
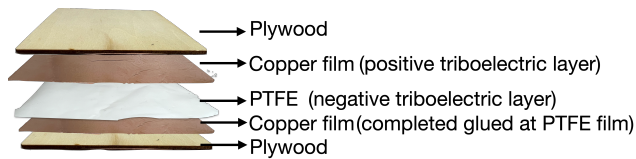

Figure 2: The structure of our vibration sensor.

The issue with this implementation, however, is that the sensor cannot survive some of the common woodworking operations, such as screwing and nailing. As a metallic object, when a screw or nail passed through the sensor, the copper electrodes became electrically connected (short-circuited), which led to no current flow within the circuit as the voltage potential equalized between the electrodes (Figure 3a). Other common operations, such as drilling or sanding, do not have this problem. While there are special types of nails coated with a non-conductive material, they are not widely used in practice, so a better solution is needed.
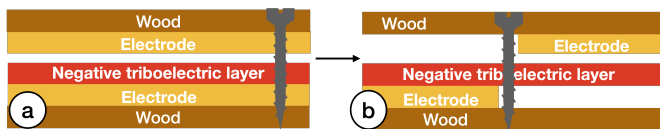

Figure 3: Side views of the sensor structure. (a) With the current design, the screw inside the sensor connects the electrodes, thus causing a short circuit. (b) The new electrode design removes the overlap between the electrodes to avoid short-circuiting. A horizontal gap between the top and bottom electrodes further avoids short-circuiting along the shared edge of the electrodes.

5 DESIGNING A MAKABLE SENSOR

The basic principle of our approach was to minimize the overlap between the electrodes. For example, instead of covering the entire PTFE film, the electrodes can be arranged to cover only half of it (Figure 3b). In the simplest way, the top and bottom electrodes can cover the right and left half of the sensor respectively. With this

arrangement, the electrodes will not be easily connected by a screw. Note that, short circuits may still happen if a screw or nail appears on the shared edge of the electrodes. The problem, however, can be avoided by separating the electrodes with a gap wider than the diameter of the screw (Figure 3b). With this design, half of the PTFE film is in contact with the wood substrate, which now also serves as the positive triboelectric layer along with the copper film on the same side.

The issue with this simple modification is that the electrode coverage could be largely uneven after the plywood is cut into parts of different shapes. A sensor with uneven electrode coverage is susceptible to environmental electromagnetic (EM) noises, thus impacting the signal-to-noise ratio (SNR). Such noise could hurt the accuracy and robustness of iWood as an activity sensor. In an ideal situation with equal electrode coverage, EM noises cause similar voltage signals on each electrode, thus can be almost canceled from each other in the output data, resulting in the minimum impact on the SNR. However, such a balance cannot be guaranteed inside a cutout. In an extreme case, where one of the electrodes is mostly cut off from the sensor (Figure 4a), the EM noises received from the opposite electrode will be largely included in the output signal, thus significantly degrading SNR. According to our test conducted under frequencies from 20Hz to 500Hz (frequency range of common user activities), the noise of a 610mm x 610mm sensor with only one electrode could be 100 times larger than the same sensor with well-balanced electrode coverage.
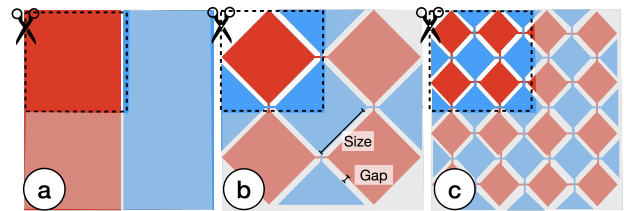

Figure 4: Top view of the iWood electrode layout. (a) The top (red) and bottom (blue) electrodes, each covering half of the sensing area. (b) iWood opts for a grid electrode layout to avoid the extremely unbalanced coverage of the electrodes in (a). (c) The same cutout containing smaller electrodes has more overlaps between the connection lines (less makeable) but less of the unbalancing issue (better SNR).

To mitigate this problem, we opted for a different electrode design. Instead of using a single piece of the electrode on each side of the PTFE film, we opted for a grid layout with diamond-shaped electrodes connected in rows and columns (Figure 4b). In our design, the top and bottom electrodes stagger with each other with a 12.7mm gap to avoid short-circuits along the shared edges. We chose 12.7mm because it is the diameter of the largest wood screw that we found on the market. This new design allows the short-circuit problem to be largely avoided without sacrificing SNR (or sensitivity). Each electrode in the grid is connected to its four neighbors through connection lines of 2mm wide. This largely preserves the disconnection of edge electrodes in a cutout of any convex shape. In a concave shape like a star, some of the edge electrodes could be

cut off from the sensor but most others will still be functional. This helps avoid the extreme unbalance situation discussed above.

Note that the connection lines from nearby electrodes on the opposite side may still overlap with each other at intersections (e.g., where the red and blue lines cross each other in Figure 4b). Screws or nails in these locations may cause short circuits. The amount of overlap is determined by the size of the electrodes. For example, layouts with larger electrodes have fewer overlaps because there are fewer connection lines and electrodes. The trade-off, however, is in the lack of ability to tolerate the unbalance issue of electrode coverage upon cutting. Thus, layouts with larger electrodes could be more susceptible to EM noises. In contrast, layouts with smaller electrodes are less problematic upon cutting but can introduce more overlaps and short-circuiting issues (Figure 4c), which is a more serious issue. Next, we describe our approach to identifying an optimal size for the electrodes.

6 SIMULATION STUDY

An optimal electrode size can be found by testing cutouts of different shapes, sizes, orientations, and locations inside a sensor. Each of these parameters has many variations, leading to numerous combinations, which makes it infeasible for the study to be conducted manually. As such, we developed software to simulate all different situations.

6.1 Software Simulator

Our software simulated cutouts in different shapes, sizes, and orientations inside a virtual sensing area of 6100mm × 6100mm wide with electrodes of different sizes and a 12.7mm gap between the electrodes. The size of the sensing area is adjustable and the one used in our study was based on the size of a plywood board commonly found in DIY and crafting stores in our region. We chose six basic shapes to cover a range of simple and complex cutouts commonly seen in woodworking projects. These include triangle, rectangle, ellipse, star, carve-out, and hole-out (Figure 5).
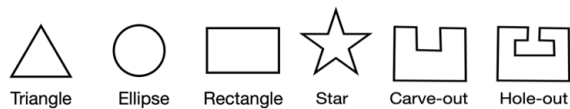

Figure 5: The six basic cutout shapes tested in the simulation.

We then varied the size of the cutouts by scaling them in the x- and y-directions six times by a factor of 1 to 6. This resulted in 36 different sizes and 30 variations of the basic shapes. The smallest cutout has a bounding box of 100 × 100mm, which is roughly the size of some of the small wooden artifacts found in our makeability study. We rotated each cutout from 0° to 180° with a step size of 22.5°. Each combination of shape × x-scale × y-scale × rotation angle was then tested at different locations inside the virtual sensor along the x- and y-axis with a step size of 5mm in each direction, except when a cutout did not fit inside the sensor (e.g., at corners). Lastly, we varied the electrode size to cover a wide range of possibilities from 10mm to 120mm wide with a step size of 10mm.

In each tested condition and for each electrode size, we calculated two scores with one indicating the probability of short-circuiting and the other one indicating the ratio between the top and bottom electrode coverage. As discussed earlier, larger electrodes tend to have fewer short-circuiting problems, but smaller electrodes tend to have better SNR. The *Short-Circuiting Probability* was calculated as the area of overlaps and any region that can be bridged by a screw of 12.7mm in diameter, divided by the area of a cutout. In our calculation, the connection lines were set as 2mm wide to be consistent with our implementation. The *Balance Ratio* was calculated as the smaller of the top and bottom electrode coverage, divided by the larger of them. When the coverage was calculated, we excluded the edge electrodes that were cut disconnected from the remainders. The *Balance Ratio* measures how well the coverages of the top and bottom connected electrodes are balanced. The higher this score is the better the coverages are balanced. In extreme cases, where electrodes on one side of a cutout are largely cut disconnected, the *Balance Ratio* will be close to zero. Thus, the *Balance Ratio* can also be used to detect the occurrence of extremely unbalanced coverage.

6.2 Result

We calculated the average Short-Circuiting Probability and aggregated them by electrode size, basic cutout shape, and cutout size in six groups: $100cm^2$, $(100, 400 \ cm^2]$, $(400, 900 \ cm^2]$, $(900, 1600 \ cm^2]$, $(1600, 2500 \ cm^2]$, and $(2500, 3600 \ cm^2])$. Figure 6 shows the Short-Circuiting Probability by electrode size, cutout shape, and cutout size group. Cutout shape and size had no observable impact on the likelihood of short-circuiting. As the size of the electrode increased, the chance for the electrodes and connection lines to be short-circuited decreased. With electrodes bigger than 80mm, the probability of short-circuiting became lower than 5%, which is very promising.
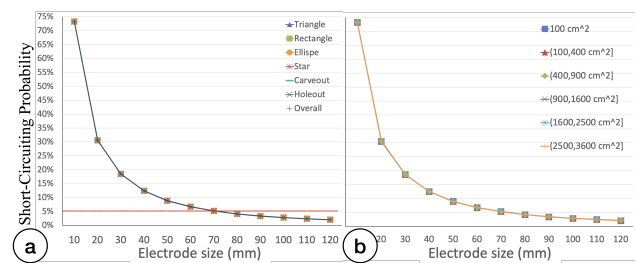

Figure 6: (a) Short-Circuiting Probability shown against electrode size and cutout shape. (b) Short-Circuiting Probability shown against electrode size and cutout size group.

Figure 7 shows the *Balance Ratio* for the electrodes larger than 80mm. As expected, the *Balance Ratio* decreased with the increase of the size of the electrodes. The data also shows that the balance ratios of the electrodes bigger than 80mm are far greater than zero, meaning that extremely unbalanced coverage is rare. Among the different cutout shapes, the star received the lowest scores. As expected, edge electrodes, especially the big ones, are more likely to be cut disconnected in a concave shape. When it happens to either electrode layer, the electrode coverage becomes largely unbalanced. The problem becomes more severe when the cutout
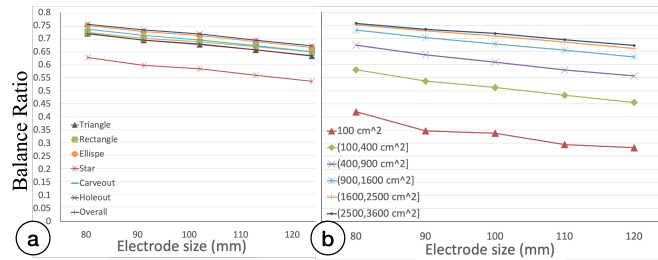
Figure 7: (a) Balance Ratio shown against electrode size and cutout shape. (b) Balance Ratio shown against electrode size and cutout size group.

is small (Figure 7b). For most other cutout shapes and sizes, the electrode coverages are relatively well balanced. Since our goal was to prioritize makeability while balancing signal clarity, we chose to use 80mm in our implementation.

7 OPTIMIZING IWOOD FABRICATION

Aside from the design of the electrode layer, the performance of iWood also depends on how the triboelectric and electrode layers are put together as a package. As discussed in Section 3, the sensitivity of iWood is mainly affected by the bonding method of the sensor layers and the material choice of the triboelectric layers. Since in our implementation, one of the electrodes also served as the positive triboelectric layer, we were also interested in learning whether the material, of which, the electrodes were made would affect sensitivity. We performed three tests to answer these questions.

7.1 Experiment Setup

Our study apparatus was implemented on a small piece of plywood board measured 100mm × 100mm wide and 5.08mm thick. Since makeability is not the focus of the studies, we only had the electrodes (100mm × 50mm) cover half of the PTFE film on each side, for the sake of simplicity. The rest of the implementation was the same as that shown in Figure 2. The electrodes were initially created using a copper film, which was later replaced by different materials along with other sensor modifications and bonding strategies based on the requirement of our tests. We created three replicated copies for each modified version to reduce the impact of fabrication variations on results.

The tests were performed in a controlled environment with the plywood sensor placed on a table. Vibration signals were generated using a vibration exciter, fixed in the center of the plywood using a high bonding double-side tape [2]. We controlled the vibration exciter [8] using a wave generator to generate sine waves of 5V, with frequencies ranging from 20Hz to 500Hz at a step size of 4.8Hz. We chose this range because it covers the vibration frequencies caused by a wide variety of user activities in daily life [39]. The voltage signal at each tested frequency was acquired using an oscilloscope. EM noises were also collected for each test condition and sensor replicas to calculate SNR. The SNR data shown in the test results are the average of all the SNRs across the tested frequencies and conditions.

7.2 Bonding Strategy

In this test, we sought to understand how the bonding method of the sensor may affect sensitivity. As mentioned earlier, there needs to be enough space for the PTFE film to bounce away from the copper film (one that also serves as the positive triboelectric layer), which means that they cannot be glued completely against each other. Therefore, a good strategy is to bond them through a small number of connection points loosely spreading across the PTFE film. Alternatively, they can be bounded through the edges connecting these points. Both approaches leave the majority of the PTFE film surface free to bounce, maximizing separation distance. In this study, we tested two bonding strategies on the sensor: (1) gluing at the four corners of the PTFE film (Figure 8a); and (2) gluing the four edges of the PTFE film (Figure 8b). We also tested these bonding methods with different types of glues and found that 3M plastic glue [1] performed the best to hold the entire unit firmly against all the woodworking operations from Study 1.

Figure 8c shows the result of this test. We found that across all the tested frequencies, the sensor was approximately 3db more sensitive when bonded through the corner points than through the edges. Therefore, we chose to use corner bonding in the remaining studies and in the implementation of our final prototype.
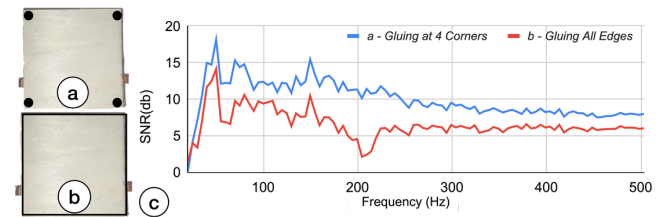

Figure 8: The prototype used in the bonding strategy test was created by: (a) gluing the copper and PTFE films together through the four corners and (b) gluing through the four edges. (c) Sensor data of the two bonding strategies.

7.3 Material Choice for the Electrodes

We conducted a second test to identify the proper material for the electrodes. Note that in our implementation, one of the electrodes also serves as the positive triboelectric layer. Therefore, it is unclear whether electrode material may affect sensitivity. To answer this question, we implemented and tested sensors with electrodes made of four different types of conductive materials: (1) copper film, (2) aluminum foils, (3) carbon coating, and (4) nickel coating (Figure 9). All of these conductive materials are low-cost and widely available on the market. Among these options, copper film and aluminum foil were used in previous research in triboelectric nanogenerators [54]. While carbon and nickel coating has not been used for the same purpose, spraying the electrodes on the plywood leads to better structural integrity [43, 55].

The result is shown in Figure 9e. The strength of the sensor signals decreased in the aluminum foil condition between 150Hz and 300Hz. There was no significant difference between all the other three electrode materials. Considering structural integrity, both carbon and nickel coating would work better for us. We used

nickel coating in the remaining studies and in the implementation of our final prototype.
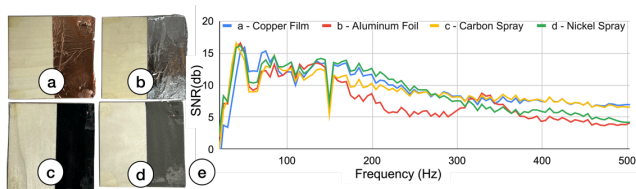

Figure 9: The prototypes used in the electrode material test were created using: (a) copper film, (b) aluminum foil, (c) carbon coating, and (d) nickel coating. (e) Sensor data of the tested electrode materials

7.4 Material Choice for the Positive Triboelectric Layer

In the third test, we compared the sensitivity of the current implementation versus a 4-layer alternative approach with a dedicated positive triboelectric layer, created using PU Wood Finish from Varathane or a nylon fabric from Urban (Figure 10b-c). Both PU coating and nylon are commonly used in triboelectric nanogenerators [54]. The PU coating has the benefit of better structural integrity for the sensor. Our result is shown in Figure 10d. SNR dropped in the PU condition. No obvious improvement could be found with a dedicated positive triboelectric layer using nylon. Therefore, we did not change the structure of the sensor to allow it to remain simple to be fabricated.
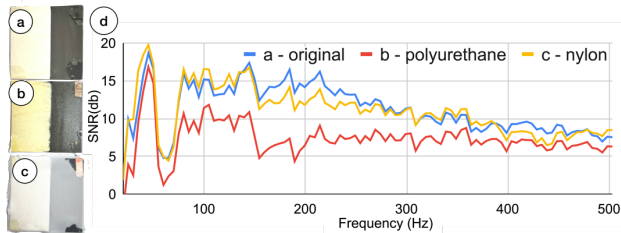

Figure 10: The prototypes used in the positive triboelectric layer test were created with: (a) no additional positive triboelectric layer, (b) a dedicated positive triboelectric layer created using (b) polyurethane, and (c) nylon. (d) Sensor data of the tested conditions

8 IMPLEMENTATION

Based on the results of the tests, we implemented the final iWood prototype. In this section, we describe our implementation details and a software pipeline for gesture and activity recognition.

8.1 Fabrication

We created the electrodes directly on the plywood substrates (610mm × 610mm) using nickel spray paint (Figure 11a). The diamond patterns for the two layers were created using acrylic stencils,

made using a laser cutter, and were fixed on top of the corresponding substrates using double-sided tape. Upon the competition of the electrode layers, the row and column connections were created using 2mm wide copper tape from Tape Master (Figure 11b). We attached a PTFE film firmly to an electrode layer and substrate with no space for bouncing. The other layer and substrate were connected using the point bonding strategy with the bonding points separated 50mm apart from each other in the x and y directions (Figure 11c). To achieve the best bonding strength, we primed the PTFE film with a plastic glue activator before the layers were put together. We created two copies of the prototype with different thicknesses (6.35mm and 12.7mm) to satisfy the need for different applications. Each prototype costs no more than 25% higher than a regular plywood board of the same size (plywood board: $20, PTFE film: $2, nickel coating: $3).
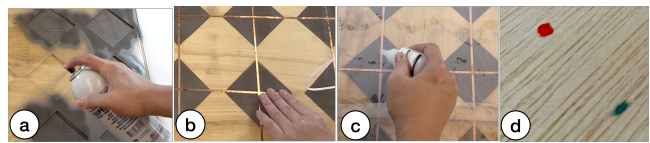

Figure 11: Illustration of the fabrication process of iWood. (a) The electrodes were created on a plywood substrate using nickel spray paint. (b) The row and column connections between the electrodes were created using a 2mm wide copper tape. (c) The electrodes and PTFE film were glued together using the point bonding strategy (d) Access points were marked on the plywood to indicate where the top (green) and bottom (red) electrodes can be reached.

To facilitate the connection to the electronics and data measurement device, we marked several access points on the plywood to indicate the location of the top (green) and bottom (red) electrodes (Figure 11d). The access points can be connected to the electronics in many different ways. For simplicity's sake, we put a small screw at one of the top and bottom access points and wired them to an Analog Discovery 2 [41]. Sensor data was sampled at 1kHz and was streamed to a laptop for processing. We believe that with technology advancement, all the other electronics components may eventually be integrated into the material [16, 57].

8.2 Signal Processing

The raw sensor data was first transformed from the time domain to the frequency domain. We then used a low-pass filter at 500Hz to remove the high-frequency components that are unlikely caused by user activities. Additionally, we performed a band-stop filter to remove the harmonic frequencies of powerline noise (i.e., 60Hz and 300Hz). Further, we performed an adaptive background subtraction to remove all the other random noises.

The input gesture or user activity in the signal data was segmented using a coarse-to-fine energy-based sliding window approach [35]. We first employed a 3-second sliding window with a 90% overlap to detect the occurrence of an event of interest. To do so, we calculated the energy of the sliding window by summarizing the square magnitude of its 256 FFT bins. If the energy was higher than a predetermined coarse-power threshold, an event was

detected. Otherwise, we moved on to the next window. Upon the detection of an event, we applied a new 0.5-second sliding window with a 75% overlap to look for the start and end of the event at a finer granularity. If the energy of a window raised above a predetermined fine-power threshold, the start of the event was identified. We then advanced the sliding window until the end of the event was found, based on the drop of energy of the window below the fine-power thread. The thresholds used in our implementation were determined using a pilot study and were left unchanged in our system evaluation.

8.3 Featurization and Machine Learning

Following a common approach used in the literature [22, 23, 56], we derived machine learning features using the segmented data in the frequency domain with a sliding window of 512 bins with a 75% overlap. We calculated max, mean, 1st quantile, median, 3rd quantile, h-mean, moment, skew, kurtosis, and standard deviation for each frequency band (256×10 values). We also computed the length of segmented data in the time domain. In total, our machine learning model was trained using 2561 features. We used a Random Forest from Scikit-learn [34] with a forest size of 100 and a maximum depth of 30. The value of these parameters was chosen to balance sensing accuracy and model complexity. We ran the classifier on a MacBook Pro.

9 DEMO PROJECTS MADE OF IWOOD

To demonstrate the capability of iWood and how new smart home applications can be enabled, we created three smart home items: a table, a nightstand, and a cutting board (Figure 12). These smart items were also used later in our system evaluation to measure the sensing accuracy of our prototype.

Figure 12: The three smart items created using iWood: (a) table, (b) nightstand, and (c) cutting board

9.1 Table.

The table consisted of four wooden legs attached to a 1220mm × 610mm × 12.7mm plywood tabletop, which was created using two iWood boards attached side-by-side (Figure 12a). Each leg came with a pre-installed 8mm hanger bolt, allowing them to be screwed to the corners of the tabletop. The smart table can be used as an extension of the input device on a phone through the detection of simple input gestures. In our implementation, the system can recognize tapping the table using the fingertip, swiping the finger against the table, knocking the table using the knuckle, and slapping it using the palm. Further, the smart table can be configured to log the routine activities or work progress of the user and respond accordingly to

enable new applications. For example, in our implementation, the table can sense events like writing, erasing, stapling, dispensing a tape, and sharpening a pencil. This information can be useful to inform the user about their work practices for personal reflection or infer the work psychological state of the user for social facilitation if unusual patterns are observed.

9.2 Nightstand.

The nightstand consisted of a top panel, a bottom panel, three side panels, four legs, and a drawer. The top panel (500mm × 500mm × 12.7mm) and drawer bottom (310mm × 375mm × 6.35mm) were created using iWood and a jigsaw (Figure 12b). The top panel was attached to the frame and side panels from the corners using four 10mm wood screws. The drawer bottom was fixed to the notch of the drawer sides using glue. As an activity sensor, the top panel can detect the user's routine task of pumping lotion for nighttime skincare. The drawer can also detect and log the user's bedtime reading habit through the detection of the user taking the book from the drawer and putting it back. If this routine breaks during a busy week before the user's school project is due, which can be detected through the work activities via the table, this change of behavior can be logged for the user to view at a later time.

9.3 Cutting board.

Like regular plywood, iWood can withstand laser cutting. We created a custom cutting board (400mm × 600mm × 6.35mm) (Figure 12c), using graphics editing software and a laser cutter. Our smart cutting board can recognize common cooking activities on it, such as chopping, slicing, meat tenderizing, stirring, grating, and rolling a rolling pin. This information can be used to augment a user's cooking experience (Figure 13). For example, a progress indicator can be shown on the user's tablet to provide a better awareness of the time left for their steak to be tenderized or the scrambled eggs to be stirred. The smart cutting board can also find applications in the automatic skill assessment, similar to prior work for working space [11, 20, 37]. For example, the user's expertise level can be analyzed based on the duration of each activity and overall food preparation time. Such automatic assessment could create opportunities for in-situ feedback, skill-level evaluation, and skill degradation detection.
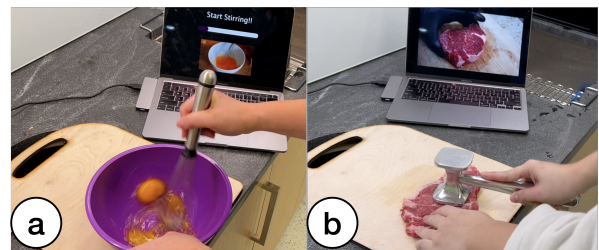

Figure 13: (a) Sensing stirring on the cutting board allows the system to show the time left for the egg to be stirred through a progress bar. (d) The system automatically pauses a cooking tutorial video when the user starts tenderizing the meat. Upon the user stops the action, the system resumes the video.

10 EVALUATION

We conducted an experiment to measure the sensing performance of the table, nightstand (top panel), and cutting board. We were interested in measuring how accurate user gestures and activities can be recognized on these items. To push the limit of our system even further, we evaluated system robustness against individual and device variances among different users and smart items, which in our case were created in different form factors with sensors in different shapes and sizes.

10.1 Participants

Ten right-handed participants (average age: 27.2, 7 males, 3 females) were recruited to participate in the study.

10.2 Gestures and Activities

Our experiment included 12 daily activities ranging from those commonly carried out on a kitchen table or cutting board, such as chopping, slicing, stirring, tenderizing, grating, and rolling a rolling pin, to those that can be carried out on a desk table or nightstand, such as writing, erasing, stapling, pumping lotion, dispensing a tape, and rotating a pencil sharpener (Figure 14). We also included four input gestures, including tapping, knocking, slapping, and swiping in any direction. The activities and gestures tested in our experiment produced vibrations varying in strength and frequency across different users and smart items.
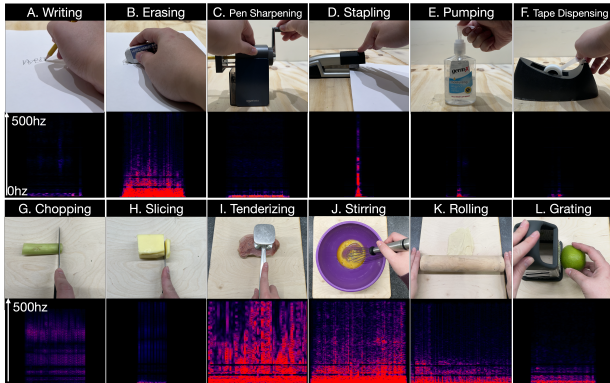

Figure 14: User activities tested in our experiment.

10.3 Data Collection

Before the experiment started, participants were given several minutes to learn the activities and gestures. During data collection, participants were asked to perform the tasks on the corresponding smart items in whatever way they felt comfortable, either in a standing or sitting position. The order of the activities, gestures, and the 10 repetitions of them were randomized for every participant. Note that not all the activities and gestures are performed on all the smart items. For example, writing may take place on the table or nightstand (e.g., writing a quick note) but not usually on a cutting board. Therefore, the data collected on the table and nightstand only included writing, erasing, stapling, pumping lotion, dispensing a tape, rotating a pencil sharpener, and all the hand

gestures. Similarly, the activities carried out on the cutting board are unlikely to occur on a nightstand. Therefore, the data collected on the cutting board (placed on a regular desk) only included chopping, slicing, stirring, tenderizing, grating, and rolling a rolling pin. We also repeated the same set of kitchen activities on the table. Repeating the same group of activities and gestures on different smart items allowed us to investigate how reliable our system can recognize them on different items.

10.4 Results

In this section, we report the performance of our prototype measured using a variety of different ways, including within-user accuracy, cross-user accuracy, mixed-item accuracy, and item identification accuracy.

10.4.1 Within-User Accuracy. Within-user accuracy was the measurement of the prediction accuracy on a specific smart item where the training and testing data were from the same user. For each participant, we conducted twofold cross-validation, where half of the data was used for training and the rest for testing.

For the gestures, the system achieved an average within-user accuracy of 93% (std: 1.4) on the table and 90.7% (std: 3.9) on the nightstand. In particular, on the table, the accuracy for *Tapping*, *Swiping*, *Knocking*, and *Slapping* was 91%, 94%, 94%, and 93% respectively. On the nightstand, the accuracy was 92%, 94%, 85%, and 92% respectively. The major source of errors came from *Knocking* and *Slapping* because sometimes participants performed *Knocking* the phalanges, which produced signals similar to that of *Slapping*.

For the activity recognition, the system achieved an overall within-user accuracy of 95.3% across all the smart items. In particular, the system achieved an average accuracy of 94.7% (std: 4.1) on the table, 93.8% (std: 3.8) on the nightstand, and 97.3% (std: 1.9) on the cutting board. Figure 15 shows the confusion matrices of the tested activities. Most activities can be recognized with high accuracy, especially within a smaller subset carried out on the cutting board or nightstand. The recognition accuracy remained high when it came to the table with more activities, suggesting that the within-participant signals were fairly consistent and robust to item variation. The only exception was the rolling pin (83%, std: 2.1), which was confused with *Stirring* more often (92%, std: 0.9). Considering the size of our training sample was relatively small, we suspect that if additional data were collected, accuracy would rebound.

10.4.2 Cross-User Accuracy. Across-user accuracy measured how well a model worked across different users. We conducted a leave-one-subject-out cross-validation by using the data from nine participants for training and the remaining one for testing. Our result showed that the cross-user accuracy for gesture recognition was 88.5% (std: 4) on the table and 85% (std: 6.1) on the nightstand. In particular, on the table, the accuracy for *Tapping*, *Swiping*, *Knocking*, and *Slapping* was 85%, 86% 89%, and 94% respectively. On the nightstand, the accuracy was 93%, 78%, 84%, and 85% respectively. Note that *Tapping* and *Swiping* caused more confusion especially when swiping was performed at a short distance.

For activity recognition, the average cross-user accuracy across all the tested items was 89.9%. In particular, the system achieved an
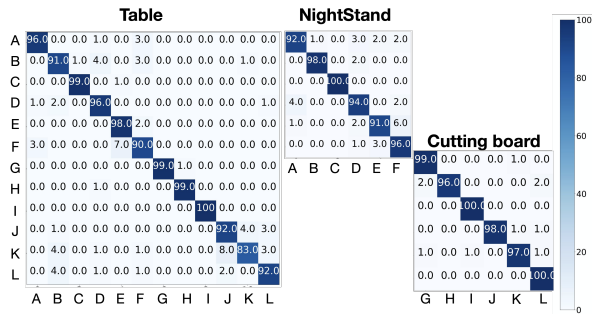
Figure 15: The confusion matrices of the within-user accuracy for activity recognition.

average cross-user accuracy of 87.8% (std: 5.5) on the table, 88.3% (std: 8.8) on the nightstand, and 93.6% (std: 1.9) on the cutting board. Figure 16 shows the confusion matrices for these items. With the inclusion of individual variance in the data, the activities with a similar motion began to get more errors. Example includes *Erasing* vs *Grating*. For the activities with more distinguishable motions, such as *Chopping* vs *Slicing*, the recognition accuracy also decreased. To understand the reason, we examined the data closely and found that some participants were faster than the others when performing the tasks due to individual differences in skill and expertise level. We see it as a strong promise of our system in skill assessment applications. Overall, despite the 5% decrease in comparison to the within-user accuracy, our system still performed reasonably well across different participants.
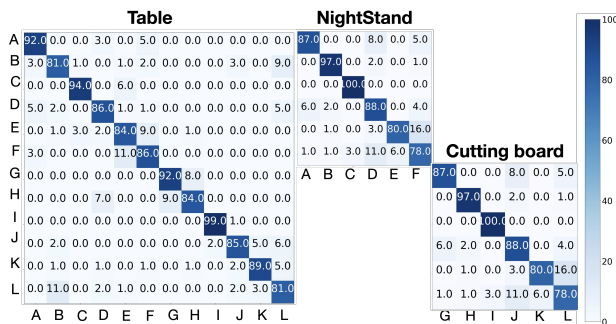

Figure 16: The confusion matrices of the cross-user accuracy for activity recognition.

10.4.3 Mixed-Item Accuracy. Mixed-item accuracy measured whether a general model can be trained for all three smart items. Our general model was trained by including all the data collected from the table, nightstand, and cutting board. The performance of the model was evaluated through (1) within-user accuracy using a twofold cross-validation and (2) cross-user accuracy using a leave-one-subject-out cross-validation.

For the input gestures, the system achieved an average within-user mixed-item accuracy of 88.3% (std: 4) and cross-user mixed-item accuracy of 86.6% (std: 5.2) (Table 1).

Table 1: the mixed-item within-user accuracy and mixed-item cross-user accuracy for four input gestures.

	Tapping	Swiping	Knocking	Slapping
Within-User Acc.	84.5%	94.0%	87.0%	88.0%
Cross-User Acc.	93.5%	84.5%	81.0%	87.5%

For activity recognition, the within-user mixed-item accuracy was 88.9% (std:7.2) and The cross-user mixed-item accuracy was 84.2% (std: 8.1). Figure 17 shows the confusion matrices for the two types of accuracies. While the general model did not perform as well as the item-specific models, it is still encouraging to see that the system remained reasonably accurate. The promise of the general model is that it avoids the need to rely on individual models to be trained separately on each smart item. A single model can be distributed to handle a subset or perhaps the entire inventory of home items. Note that if we removed the most confusing activities, Pumping, Tape Dispensing, Slicing, and Grating, the within- and cross-user mixed-item accuracies rebounded to 91.3% (std: 5.4) and 91.4% (std: 6.0) respectively.
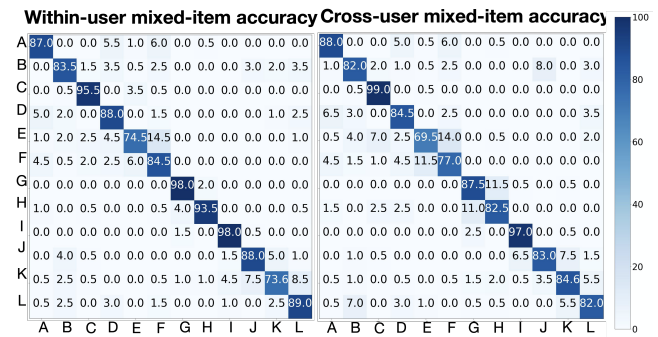

Figure 17: The confusion matrices of mixed-item accuracy.

10.4.4 Smart Item Detection. We also investigated if a model could be trained to infer the identity of an item based on the input signal. We measured the item detection accuracy using a twofold cross-validation with the dataset composed of all the gestures and activities. Our result yielded an overall accuracy of 90.1%. Particularly, the item detection accuracy was 90.1% using the activity data and 96.1% using the gesture data. The result suggests that it is possible to identify a smart item based on its unique vibration signature caused by different types of activities and input gestures. This is encouraging even though our experiment only included three items. In many usage scenarios, especially when there are duplications of an existing item, such self-awareness allows the system to automatically adapt a proper item-specific model to better recognize input or contextual events on that item.

11 LIMITATIONS AND FUTURE WORK

We present insights learned from this work, discuss the limitations of our prototype, and propose future research.

11.1 Short-circuiting

Our implementation minimizes the chance of short-circuiting to around 5% but when a short circuit occurs, the sensor malfunctions. This can be an issue, especially after the completion of the assembly of a smart item. As a part of our future research, we will explore solutions to eliminate the short-circuiting issue. We will develop tools to enable automatic detection of short-circuiting when woodworking operations are carried out. We will also create tools to allow easy diagnosis, debugging, and visualization of the status of the sensing system.

11.2 Composition of two or more interactive plywood parts

Our current work investigated smart objects and items composed of a single piece of iWood or two disconnected ones. In many usage scenarios, multiple interactive plywood boards may need to be connected to create a larger item, such as a floor, thus new challenges will arise. Future research needs to investigate tools that could allow the connections to be made easier (e.g., via the side) in series or parallel.

11.3 Robust Vibration Sensing.

Like other approaches using vibration sensing [29, 39, 56], sensor signals change with the presence of additional objects but such change may not impact recognition accuracy. For example, our system can detect the activities with the presence of additional objects (e.g. laptop, stapler) though it was trained with activities carried out on an empty table. This, however, may not be true with a different set of activities or objects. Future research will investigate how sensing accuracy will be affected and ways to mitigate negative impacts.

11.4 Sensing 2D information.

When multiple pieces of iWood are arranged in a 2D space, coarse-grained 2D information can be sensed if the sensors are connected in parallel. This way, each iWood serves as a pixel of a larger sensing area. An alternative approach is to enable 2D sensing on individual iWood sensors. This will allow finer-grained 2D information to be sensed, which could enable a broader range of new applications. As a part of our plan to continue this work, we will extend the current implementation of iWood to sensing 2D information. This will involve redesigning the structure and electrode layout of the sensor.

12 CONCLUSION

Through a new interactive plywood prototype, we explored how a smart physical world comprised of wooden furniture and kitchen items could be created in the future using the established methods and woodworking operations, by which, the current physical world is created. We advocate the notion of makeability as an inescapable consideration when developing interactive materials. We argue that in the new era of ubiquitous computing, interactivity and computing should be treated as materials' digital properties, which adds to the already existing natural properties, such as stiffness and conductivity. To smoothly blend the digital and physical worlds, we propose that a material's digital properties should be inheritable by anything that is made of this material. We demonstrated through iWood that its ability to sense vibration can be inherited by three household items made of it, including a table, nightstand, and cutting board. With vibration sensing, these items can now detect a variety of user activities and input, while still being able to largely preserve the look and feel of their non-computational counterparts. We believe that our research may serve as an important groundwork for the future development of computational materials and smart environments.

ACKNOWLEDGMENTS

REFERENCES

[1] MTM Scotch-WeldTM Plastic & Rubber Instant Adhesive PR40 | 3M United States: https://www.3m.com/3M/en_US/p/d/b40066945/. Accessed: 2022-03-29.

[2] MTM VHBTM Adhesive Transfer Tape F9473PC: https://www.3m.com/3M/en_US/p/d/b40071700/. Accessed: 2022-03-29.

[3] Gregory D. Abowd 2020. The Internet of Materials: A Vision for Computational Materials. IEEE Pervasive Computing. 19, 2 (Apr. 2020), 56–62. DOI:https://doi.org/10.1109/MPRV.2020.2982475.

[4] An aeroelastic flutter based triboelectric nanogenerator as a self-powered active wind speed sensor in harsh environment - ScienceDirect: https://www.sciencedirect.com/science/article/abs/pii/S2352431617300780. Accessed: 2022-03-29.

[5] Nivedita Arora, Ali Mirzazadeh, Injoo Moon, Charles Ramey, Yuhui Zhao, Daniela C. Rodriguez, Gregory D. Abowd, and Thad Starner 2021. MARS: Nano-Power Battery-free Wireless Interfaces for Touch, Swipe and Speech Input. The 34th Annual ACM Symposium on User Interface Software and Technology (New York, NY, USA, Oct. 2021), 1305–1325.

[6] Nivedita Arora, Steven L. Zhang, Fereshteh Shahmiri, Diego Osorio, Yi-Cheng Wang, Mohit Gupta, Zhengjun Wang, Thad Starner, Zhong Lin Wang, and Gregory D. Abowd 2018. SATURN: A Thin and Flexible Self-powered Microphone Leveraging Triboelectric Nanogenerator. Proceedings of the ACM on Interactive, Mobile, Wearable and Ubiquitous Technologies. 2, 2 (Jul. 2018), 60:1-60:28. DOI:https://doi.org/10.1145/3214263.

[7] Jun Chen, Guang Zhu, Weiqing Yang, Qingshen Jing, Peng Bai, Ya Yang, Te-Chien Hou, and Zhong Lin Wang 2013. Harmonic-resonator-based triboelectric nanogenerator as a sustainable power source and a self-powered active vibration sensor. Advanced Materials (Deerfield Beach, Fla.). 25, 42 (Nov. 2013), 6094–6099. DOI:https://doi.org/10.1002/adma.201302397.

[8] Dayton Audio - DAEX25 Sound Exciter Pair: https://www.daytonaudio.com/product/1087/daex25-sound-exciter-pair. Accessed: 2022-03-29.

[9] Artem Dementyev, Hsin-Liu (Cindy) Kao, and Joseph A. Paradiso 2015. Sensor-Tape: Modular and Programmable 3D-Aware Dense Sensor Network on a Tape. Proceedings of the 28th Annual ACM Symposium on User Interface Software & Technology (New York, NY, USA, 2015), 649–658.

[10] Feasibility of Using Floor Vibration to Detect Human Falls - PMC: https://www.ncbi.nlm.nih.gov/pmc/articles/PMC7795781/. Accessed: 2022-03-29.

[11] Jun Gong, Fraser Anderson, George Fitzmaurice, and Tovi Grossman 2019. Instrumenting and Analyzing Fabrication Activities, Users, and Expertise. Proceedings of the 2019 CHI Conference on Human Factors in Computing Systems (New York, NY, USA, May 2019), 1–14.

[12] Jun Gong, Yu Wu, Lei Yan, Teddy Seyed, and Xing-Dong Yang 2019. Tessutivo: Contextual Interactions on Interactive Fabrics with Inductive Sensing. Proceedings of the 32nd Annual ACM Symposium on User Interface Software and Technology (New York, NY, USA, Oct. 2019), 29–41.

[13] Nan-Wei Gong, Jürgen Steimle, Simon Olberding, Steve Hodges, Nicholas Edward Gillian, Yoshihiro Kawahara, and Joseph A. Paradiso 2014. PrintSense: a versatile sensing technique to support multimodal flexible surface interaction. Proceedings of the SIGCHI Conference on Human Factors in Computing Systems (New York, NY, USA, Apr. 2014), 1407–1410.

[14] Saifei Hao, Jingyi Jiao, Yandong Chen, Zhong Lin Wang, and Xia Cao 2020. Natural wood-based triboelectric nanogenerator as self-powered sensing for smart homes and floors. Nano Energy. 75, (Sep. 2020), 104957. DOI:https://doi.org/10.1016/j.nanoen.2020.104957.

[15] Chris Harrison and Scott E. Hudson 2008. Scratch input: creating large, inexpensive, unpowered and mobile finger input surfaces. Proceedings of the 21st annual ACM symposium on User interface software and technology (New York,

NY, USA, Oct. 2008), 205–208.

[16] Pei He, Jianyun Cao, Hui Ding, Xin Zhao, and Zheling Li 2020. 16 - Electronic devices based on solution-processed two-dimensional materials. Synthesis, Modeling, and Characterization of 2D Materials, and Their Heterostructures. E.-H. Yang, D. Datta, J. Ding, and G. Hader, eds. Elsevier. 351–384.

[17] David Holman and Roel Vertegaal 2011. TactileTape: Low-Cost Touch Sensing on Curved Surfaces. Proceedings of the 24th Annual ACM Symposium Adjunct on User Interface Software and Technology (New York, NY, USA, 2011), 17–18.

[18] Lasse Kaila, Henrik Raula, Miika Valtonen, and Karri Palovuori 2012. Living wood: a self-hiding calm user interface. Proceeding of the 16th International Academic MindTrek Conference (New York, NY, USA, Oct. 2012), 267–274.

[19] Mustafa Emre Karagozler, Ivan Poupyrev, Gary K. Fedder, and Yuri Suzuki 2013. Paper generators: harvesting energy from touching, rubbing and sliding. Proceedings of the 26th annual ACM symposium on User interface software and technology (New York, NY, USA, Oct. 2013), 23–30.

[20] Aftab Khan, Sebastian Mellor, Eugen Berlin, Robin Thompson, Roisin McNaney, Patrick Olivier, and Thomas Plötz 2015. Beyond activity recognition: skill assessment from accelerometer data. Proceedings of the 2015 ACM International Joint Conference on Pervasive and Ubiquitous Computing (New York, NY, USA, Sep. 2015), 1155–1166.

[21] Weon-Guk Kim, Do-Wan Kim, Il-Woong Tcho, Jin-Ki Kim, Moon-Seok Kim, and Yang-Kyu Choi 2021. Triboelectric Nanogenerator: Structure, Mechanism, and Applications. ACS Nano. 15, 1 (Jan. 2021), 258–287. DOI:https://doi.org/10.1021/acsnano.0c09803.

[22] Gierad Laput, Karan Ahuja, Mayank Goel, and Chris Harrison 2018. Ubicoustics: Plug-and-Play Acoustic Activity Recognition. Proceedings of the 31st Annual ACM Symposium on User Interface Software and Technology (New York, NY, USA, Oct. 2018), 213–224.

[23] Gierad Laput, Eric Brockmeyer, Scott E. Hudson, and Chris Harrison 2015. Acoustruments: Passive, Acoustically-Driven, Interactive Controls for Handheld Devices. Proceedings of the 33rd Annual ACM Conference on Human Factors in Computing Systems (New York, NY, USA, Apr. 2015), 2161–2170.

[24] Long Lin, Sihong Wang, Simiao Niu, Chang Liu, Yannan Xie, and Zhong Lin Wang 2014. Noncontact Free-Rotating Disk Triboelectric Nanogenerator as a Sustainable Energy Harvester and Self-Powered Mechanical Sensor. ACS Applied Materials & Interfaces. 6, 4 (Feb. 2014), 3031–3038. DOI:https://doi.org/10.1021/am405637s.

[25] Long Lin, Yannan Xie, Sihong Wang, Wenzhuo Wu, Simiao Niu, Xiaonan Wen, and Zhong Lin Wang 2013. Triboelectric Active Sensor Array for Self-Powered Static and Dynamic Pressure Detection and Tactile Imaging. ACS Nano. 7, 9 (Sep. 2013), 8266–8274. DOI:https://doi.org/10.1021/nn4037514.

[26] Jian Liu, Yingying Chen, and Marco Gruteser 2016. Sensing on ubiquitous surfaces via vibration signals: poster. Proceedings of the 22nd Annual International Conference on Mobile Computing and Networking (New York, NY, USA, Oct. 2016), 424–425.

[27] Simon Olberding, Nan-Wei Gong, John Tiab, Joseph A. Paradiso, and Jürgen Steimle 2013. A Cuttable Multi-Touch Sensor. Proceedings of the 26th Annual ACM Symposium on User Interface Software and Technology (New York, NY, USA, 2013), 245–254.

[28] Alex Olwal and Artem Dementyev 2021. Hidden Interfaces for Ambient Computing: Interacting with High-brightness Visuals through Everyday Materials. Extended Abstracts of the 2021 CHI Conference on Human Factors in Computing Systems. Association for Computing Machinery. 1–5.

[29] Shijia Pan, Ceferino Gabriel Ramirez, Mostafa Mirshekari, Jonathon Fagert, Albert Jin Chung, Chih Chi Hu, John Paul Shen, Hae Young Noh, and Pei Zhang 2017. SurfaceVibe: Vibration-Based Tap amp; Swipe Tracking on Ubiquitous Surfaces. 2017 16th ACM/IEEE International Conference on Information Processing in Sensor Networks (IPSN) (Apr. 2017), 197–208.

[30] Patrick Parzer, Florian Perteneder, Kathrin Probst, Christian Rendl, Joanne Leong, Sarah Schuetz, Anita Vogl, Reinhard Schwoediauer, Martin Kaltenbrunner, Siegfried Bauer, and Michael Haller 2018. RESi: A Highly Flexible, Pressure-Sensitive, Imperceptible Textile Interface Based on Resistive Yarns. Proceedings of the 31st Annual ACM Symposium on User Interface Software and Technology (New York, NY, USA, Oct. 2018), 745–756.

[31] Patrick Parzer, Adwait Sharma, Anita Vogl, Jürgen Steimle, Alex Olwal, and Michael Haller 2017. SmartSleeve: Real-time Sensing of Surface and Deformation Gestures on Flexible, Interactive Textiles, using a Hybrid Gesture Detection Pipeline. Proceedings of the 30th Annual ACM Symposium on User Interface Software and Technology (New York, NY, USA, Oct. 2017), 565–577.

[32] Ivan Poupyrev, Nan-Wei Gong, Shiho Fukuhara, Mustafa Emre Karagozler, Carsten Schwesig, and Karen E. Robinson 2016. Project Jacquard: Interactive Digital Textiles at Scale. Proceedings of the 2016 CHI Conference on Human Factors in Computing Systems (New York, NY, USA, May 2016), 4216–4227.

[33] Thomas Preindl, Cedric Honnet, Andreas Pointner, Roland Aigner, Joseph A. Paradiso, and Michael Haller 2020. Sonoflex: Embroidered Speakers Without Permanent Magnets. Proceedings of the 33rd Annual ACM Symposium on User Interface Software and Technology. Association for Computing Machinery. 675–685.

[34] scikit-learn: machine learning in Python — scikit-learn 1.0.2 documentation: https://scikit-learn.org/stable/. Accessed: 2022-03-29.

[35] Fereshteh Shahmiri, Chaoyu Chen, Anandghan Waghmare, Dingtian Zhang, Shivan Mittal, Steven L. Zhang, Yi-Cheng Wang, Zhong Lin Wang, Thad E. Starner, and Gregory D. Abowd 2019. Serpentine: A Self-Powered Reversibly Deformable Cord Sensor for Human Input. Proceedings of the 2019 CHI Conference on Human Factors in Computing Systems (New York, NY, USA, May 2019), 1–14.

[36] Smart Floor with Integrated Triboelectric Nanogenerator As Energy Harvester and Motion Sensor | ACS Applied Materials & Interfaces: https://pubs.acs.org/doi/abs/10.1021/acsami.7b08526. Accessed: 2022-03-29.

[37] Todor Stojanov and Xue-Mei Ding 2015. Operators Skill Level Evaluation Method for Balancing of an Apparel Assembly Line. International Journal of Productivity Management and Assessment Technologies. 3, 1 (Jan. 2015), 1–12.

[38] Jianguo Sun, Kunkun Tu, Simon Büchele, Sophie Marie Koch, Yong Ding, Shivaprakash N. Ramakrishna, Sandro Stucki, Hengyu Guo, Changsheng Wu, Tobias Keplinger, Javier Pérez-Ramírez, Ingo Burgert, and Guido Panzarasa 2021. Functionalized wood with tunable tribopolarity for efficient triboelectric nanogenerators. Matter. 4, 9 (Sep. 2021), 3049–3066. DOI:https://doi.org/10.1016/j.matt.2021.07.022.

[39] Saiganesh Swaminathan, Jonathon Fagert, Michael Rivera, Andrew Cao, Gierad Laput, Hae Young Noh, and Scott E. Hudson 2020. OptiStructures: Fabrication of Room-Scale Interactive Structures with Embedded Fiber Bragg Grating Optical Sensors and Displays. Proceedings of the ACM on Interactive, Mobile, Wearable and Ubiquitous Technologies. 4, 2 (Jun. 2020), 50:1-50:21. DOI:https://doi.org/10.1145/3397310.

[40] Ryo Takahashi, Takuya Sasatani, Fuminori Okuya, Yoshiaki Narusue, and Yoshihiro Kawahara 2018. Design of Cuttable Wireless Power Transfer Sheet. Proceedings of the 2018 ACM International Joint Conference and 2018 International Symposium on Pervasive and Ubiquitous Computing and Wearable Computers (New York, NY, USA, Oct. 2018), 456–459.

[41] USB Oscilloscope and Logic Analyzer - Digilent Analog Discovery 2: https://digilent.com/shop/analog-discovery-2-100ms-s-usb-oscilloscope-logic-analyzer-and-variable-power-supply/. Accessed: 2022-04-04.

[42] Mark Weiser 1999. The computer for the 21st century. ACM SIGMOBILE Mobile Computing and Communications Review. 3, 3 (Jul. 1999), 3–11. DOI:https://doi.org/10.1145/329124.329126.

[43] Michael Wessely, Ticha Sethapakdi, Carlos Castillo, Jackson C. Snowden, Ollie Hanton, Isabel P. S. Qamar, Mike Fraser, Anne Roudaut, and Stefanie Mueller 2020. Sprayable User Interfaces: Prototyping Large-Scale Interactive Surfaces with Sensors and Displays. Proceedings of the 2020 CHI Conference on Human Factors in Computing Systems. Association for Computing Machinery. 1–12.

[44] Michael Wessely, Theophanis Tsandilas, and Wendy E. Mackay 2018. Shape-Aware Material: Interactive Fabrication with ShapeMe. Proceedings of the 31st Annual ACM Symposium on User Interface Software and Technology (New York, NY, USA, Oct. 2018), 127–139.

[45] Raphael Wimmer and Patrick Baudisch 2011. Modular and Deformable Touch-Sensitive Surfaces Based on Time Domain Reflectometry. Proceedings of the 24th Annual ACM Symposium on User Interface Software and Technology (New York, NY, USA, 2011), 517–526.

[46] Te-Yen Wu, Shutong Qi, Junchi Chen, MuJie Shang, Jun Gong, Teddy Seyed, and Xing-Dong Yang 2020. Fabriccio: Touchless Gestural Input on Interactive Fabrics. Proceedings of the 2020 CHI Conference on Human Factors in Computing Systems (New York, NY, USA, Apr. 2020), 1–14.

[47] Te-Yen Wu, Lu Tan, Yuji Zhang, Teddy Seyed, and Xing-Dong Yang 2020. Capacitivo: Contact-Based Object Recognition on Interactive Fabrics using Capacitive Sensing. Proceedings of the 33nd Annual ACM Symposium on User Interface Software and Technology (New York, NY, USA, 2020).

[48] Te-Yen Wu, Zheer Xu, Xing-Dong Yang, Steve Hodges, and Teddy Seyed 2021. Project Tasca: Enabling Touch and Contextual Interactions with a Pocket-Based Textile Sensor. Proceedings of the 2021 CHI Conference on Human Factors in Computing Machines. Association for Computing Machinery.

[49] Robert Xiao, Greg Lew, James Marsanico, Divya Hariharan, Scott Hudson, and Chris Harrison 2014. Toffee: enabling ad hoc, around-device interaction with acoustic time-of-arrival correlation. Proceedings of the 16th international conference on Human-computer interaction with mobile devices & services (New York, NY, USA, Sep. 2014), 67–76.

[50] Minyi Xu, Peihong Wang, Steven L. Zhang, Aurelia Chi Wang, Chunli Zhang, Zhengjun Wang, Xinxiang Pan, Zhong Lin Wang, and Yi-Cheng Wang 2018. A Soft and Robust Spring Based Triboelectric Nanogenerator for Harvesting Arbitrary Directional Vibration Energy and Self-Powered Vibration Sensing. Advanced Energy Materials. 8, 9 (Mar. 2018), 1–9. DOI:https://doi.org/10.1002/aenm.201702432.

[51] Po-Kang Yang, Zong-Hong Lin, Ken C. Pradel, Long Lin, Xiuhan Li, Xiaonan Wen, Jr-Hau He, and Zhong Lin Wang 2015. Paper-Based Origami Triboelectric Nanogenerators and Self-Powered Pressure Sensors. ACS Nano. 9, 1 (Jan. 2015), 901–907. DOI:https://doi.org/10.1021/nn506631t.

[52] He Zhang, Linjie Yao, Liwei Quan, and Xianglong Zheng 2020. Theories for triboelectric nanogenerators: A comprehensive review. Nanotechnology Reviews.

9, 1 (Jan. 2020), 610–625. DOI:https://doi.org/10.1515/ntrev-2020-0049.

[53] Hulin Zhang, Ya Yang, Yuanjie Su, Jun Chen, Katherine Adams, Sangmin Lee, Chenguo Hu, and Zhong Lin Wang 2014. Triboelectric Nanogenerator for Harvesting Vibration Energy in Full Space and as Self-Powered Acceleration Sensor. Advanced Functional Materials. 24, 10 (2014), 1401–1407. DOI:https://doi.org/10.1002/adfm.201302453.

[54] Renyun Zhang and Håkan Olin 2020. Material choices for triboelectric nano-generators: A critical review. EcoMat. 2, 4 (2020), e12062. DOI:https://doi.org/10.1002/eom2.12062.

[55] Yang Zhang, Gierad Laput, and Chris Harrison 2017. Electrick: Low-Cost Touch Sensing Using Electric Field Tomography. Proceedings of the 2017 CHI Conference on Human Factors in Computing Systems. Association for Computing Machinery. 1–14.

[56] Yang Zhang, Gierad Laput, and Chris Harrison 2018. Vibrosight: Long-Range Vibrometry for Smart Environment Sensing. Proceedings of the 31st Annual ACM Symposium on User Interface Software and Technology (New York, NY, USA, Oct. 2018), 225–236.

[57] Ute Zschieschang and Hagen Klauk 2019. Organic transistors on paper: a brief review. Journal of Materials Chemistry C. 7, 19 (May 2019), 5522–5533. DOI:https://doi.org/10.1039/C9TC00793H.